Supporting Information

Halevy et al. 10.1073/pnas.1109444108

SI Methods

1. Extraction and Purification. We performed three stepped phosphoric acid digestions of gently crushed bulk Allan Hills 84001 (ALH84001) at a temperature of 90 ± 1 °C, each consisting of three digestion steps. The aliquot weights were approximately 320, 1,625, and 1,550 mg (henceforth A, B, and C, respectively). The samples were loaded into glass boats, placed in the experimental apparatus (Fig. S1) and pumped down under vacuum for more than 16 h before being dropped into the acid. The CO_2 evolved from acid digestion was continuously trapped in a glass U trap immersed in liquid N_2, passing first through a coiled glass trap immersed in an ethanol–dry ice slush (approximately −75 °C) to remove water.

When a reaction step was complete (after 1, 4, and 12 h), the gas in the U trap was pumped over to remove noncondensible gases, passed through a coiled trap immersed in a pentane slush (approximately −125 °C) to remove trace contaminants (SO_2 and some organic molecules), and frozen into a valved glass sample vial immersed in liquid N_2. The sample vials were immediately taken to analysis. The analyte CO_2 was carried on a helium flow through 0.3 m of ¼″ outer diameter quartz tube packed with silver wool to remove H_2S and then through 2.5 m of ⅛″ outer diameter stainless steel column packed with Supelco Porapak-Q™ (porous polymer adsorbent) and held at −20 °C to remove water and miscellaneous contaminants. The cleaning steps described above were tested on standards of known bulk and clumped isotopic composition and found not to affect the measured isotopic values.

2. Microvolume Measurements, Standardization, and Error Estimates. The isotopic composition of CO_2 was measured on a Thermo Finnigan MAT 253 gas source isotope ratio mass spectrometer configured to measure masses 44 through 49 (1). The amounts of evolved gas were too small for reliable clumped isotope measurements in dual-inlet mode. To overcome this we installed two nearly identical 10-cm long electroformed nickel tubes with an outer diameter of 0.06125″ and an inner diameter of 0.02″ (henceforth microvolume) on the sample and reference side (Fig. S2*A*). The tubing material was chosen to minimize surface area and reactivity. The sample gas was frozen into the sample-side microvolume by immersion in liquid N_2 and subsequently thawed in the microvolume alone (excluding the bellows or any other tubing). The pressure in the microvolume allowed several reliable clumped isotope data acquisitions before the gas ran out. A similar pressure was reached in the reference-side microvolume by compressing the reference-side bellows and closing off the reference-side microvolume from the bellows. The reference-side bellows were adjusted after every acquisition to match the pressure of the gas remaining in the sample-side microvolume. The pressure on the sample and reference side was, in general, balanced within 1.5% and mostly within <0.8%.

Microvolume measurements of standard materials of known bulk and clumped isotopic composition revealed a drift in the measured $\delta^{18}O$, $\delta^{13}C$, and Δ_{47} relative to low-pressure dual-inlet measurements of the same materials (Fig. S2 *B–D*). The $\delta^{18}O$ became progressively heavier in all experiments by as much as 2‰, whereas the $\delta^{13}C$ became either heavier, lighter, or remained nearly constant (within measurement error). The drift in $\delta^{13}C$ was at most a few tenths of a *permil*. The drift in $\delta^{18}O$ and $\delta^{13}C$ may be related to CO_2 vapor pressure effects, which produce large oxygen isotope fractionations but only very modest carbon isotope fractionations (2). The sample CO_2 was frozen into the microvolume and, once thawed, was free to flow through a capillary tube toward the ion source. As a result, the $\delta^{18}O$ of the first CO_2 to be measured was low relative to its bulk value and became higher during subsequent acquisitions, until stabilizing at a value slightly higher than the bulk value, due to the isotopically light material that was lost early in the measurement. The known $\delta^{18}O$ and $\delta^{13}C$ of the standard materials was retrieved by calculating an average of the $\delta^{18}O$ and $\delta^{13}C$ measured out of the microvolume, weighted by the average voltage (on the faraday cup measuring mass 44 CO_2) of each acquisition (Fig. S2 *B–D*). A small offset remained from the values measured in dual-inlet mode for both $\delta^{18}O$ and $\delta^{13}C$ (Table S1). After correction for this offset, the 95% confidence interval on the remaining error was ±0.281‰ and ±0.072‰ for $\delta^{18}O$ and $\delta^{13}C$, respectively, for the period of extraction B and ±0.159‰ and ±0.024‰, respectively, for the period of extraction C. This provides an upper limit on the measurement error in $\delta^{18}O$ and $\delta^{13}C$ instead of a formal error estimate, which here tends to grossly overestimate the error. During the period of extraction A this standardization had not yet been implemented and so no empirical error estimates exist for this period.

The raw measured value of Δ_{47} was corrected to a "heated gas" reference frame, as established in previous clumped isotope studies (1). This correction is essentially a subtraction of a composition-dependent value from the raw Δ_{47}. The correction is a linear function of δ_{47}, even up to the very high values of δ_{47} observed in ALH84001 (approximately 50‰; Fig. S3). After this correction, the value of Δ_{47} of small samples was found to be positively offset from the true known value. It is not known how clumped isotopologues behave in CO_2 ice/vapor systems, but this increase in Δ_{47} of small samples occurs also for samples that had not been frozen into a microvolume, suggesting that an additional process may be involved. The notion that something other than measurement out of a microvolume is responsible for the offset is supported also by the observation that the weighted average of Δ_{47} measured out of a microvolume was always lower (closer to the true value) than the values measured at low pressure in dual-inlet mode. The reason for this offset may be related to scrambling in the ion source, a constant background ion flux, a sample size, and reaction duration-dependent contamination acquired during the extraction, or some combination of these and other factors. An extensive set of experiments on small amounts of standards of known bulk and clumped isotopic composition did not unambiguously reveal the source of the offset, but showed it to be predictable and correctable. In the weeks before and after the extraction of aliquots B and C we subjected carbonate standards of known Δ_{47} to exactly the same extraction, purification, and measurement procedures as the ALH84001 carbonates and recorded the offset from the true value (Table S1). The offsets were averaged and this average value subtracted from the values of Δ_{47} measured for the ALH84001 carbonates. The absolute value of the remaining error on the Δ_{47} of standards treated in the same way was averaged and two standard deviations were added to give a 95% confidence interval on the error remaining after such treatment. The Δ_{47} values reported for extractions B and C are in error from the true value by ±0.039‰ and ±0.027‰, respectively. As with the bulk isotopic composition, no empirical error estimates exist for Δ_{47} during the period of extraction A, as the standardization had not yet been applied.

A second error estimate for Δ_{47} was derived from the counting statistics limit to precision. For the first and second steps (0–1 and 1–4 h, respectively) in extractions B and C, this error is smaller than the error based on standards of known composition, de-

scribed above. For the third steps in these extractions (4–12 h), the counting statistics error is larger. In all cases the larger of the two error estimates is the one reported (Table S2). For extraction of aliquot A, only the counting statistics limit is reported, as the error estimation based on standards of known composition had not yet been developed and applied. In combination with the much smaller size of aliquot A (approximately 5–6 times smaller than aliquots B and C), the less well-developed extraction and purification procedure, and the absence of experience making microvolume measurements at that time, we have much more confidence in the results obtained from extraction of aliquots B and C. We focus on these in the main text, but report the values measured from extraction of aliquot A in Table S2.

3. Treatment of Anomalous Oxygen Isotope Composition of ALH84001 Carbonates. The carbonates in ALH84001 have mass-anomalous oxygen isotopic compositions, with $\Delta^{17}O$ of approximately 0.8‰ (3). To account for this, we used the raw ratios of mass 45 and 46 CO_2 to mass 44 CO_2 (^{45}R and ^{46}R, respectively) to solve the following three equations for the samples' isotopic ratios ^{13}R, ^{17}R, and ^{18}R ($^{13}C/^{12}C$, $^{17}O/^{16}O$, and $^{18}O/^{16}O$, respectively):

$$^{45}R = {}^{13}R + 2{}^{17}R, \quad \text{[S1]}$$

$$^{46}R = 2{}^{18}R + 2{}^{13}R{}^{17}R + {}^{17}R^2, \quad \text{[S2]}$$

$$^{17}R = K_1 {}^{18}R^{\lambda} + K_2, \quad \text{[S3]}$$

where $K_1 = {}^{17}R_{VSMOW}/({}^{18}R_{VSMOW})^{\lambda}$, $K_2 = {}^{17}R_{VSMOW} \times \Delta^{17}O/1{,}000$, λ is the slope of the oxygen isotope mass-fractionation line, and $^{1x}R_{VSMOW}$ is the ratio $^{1x}O/^{16}O$ in VSMOW (Vienna Standard Mean Ocean Water). These values of ^{13}R, ^{17}R, and ^{18}R were then used to calculate the random distribution of the heavy isotopes, which was used in the calculation of Δ_{47}. With a $\Delta^{17}O$ of 0.8‰, the Δ_{47} increased by approximately 0.035‰, corresponding to a temperature decrease of approximately 7 °C (relative to the same calculation carried out with $\Delta^{17}O$ of 0‰). The samples' $\delta^{18}O$ and $\delta^{13}C$ typically increased by approximately 0.027 and approximately 0.24‰, respectively.

4. Major Element Composition Estimates. The microprobe $\delta^{18}O$ and $\delta^{13}C$ data (4–7) were correlated by Mg content in six bins of Mg normalized mole fraction (X_{Mg}), each with a width of 0.1. The average and two standard deviations of the $\delta^{18}O$ and $\delta^{13}C$ in each of the six bins are shown in Fig. 4 in the main text (gray crosses). A weighted total least squares linear fit with 95% confidence bounds is also shown in Fig. 4. We used this fit, together with the $\delta^{18}O$—major element composition data to generate a synthetic dataset consisting of 10^6 points, as follows: Combinations of $\delta^{18}O$-X_{Mg}-X_{Fe}-X_{Ca} were picked at random from a pool of 109 ion–microprobe measurements (4–6). A normally distributed random component of up to ±20% of the microprobe values was added to all four values. A value of $\delta^{13}C$ was generated using the fit described above, and a normally distributed random component of ±20% was added to its value. The synthetic data were then used to calculate a probable combination of X_{Mg}, X_{Fe}, X_{Ca} given the $\delta^{18}O$ and $\delta^{13}C$ measured in our bulk carbonate acid digestions (Fig. 1 in the main text).

5. Isotopic Evolution Model. The observed carbon, oxygen, and Δ_{47} data are most consistent with precipitation at near-constant temperature (see main text, Fig. 2, and *SI Text* section *Reliability of Temperature Determination*). Additionally, anomalous oxygen and sulfur isotope signatures in ALH84001 indicate a surface source for the fluids from which the carbonates (and sulfides) formed, but the evolution of $\delta^{13}C$ implies poor communication with the atmosphere during carbonate precipitation (see main text). We used these observations to develop a quantitative model of carbonate precipitation in ALH84001.

For reasons of carbonate chemistry, a solution sourced at the surface is likely to have a ratio of H_2O to CO_2 exceeding 10^3. For example, even if the ancient Martian atmosphere contained 1 bar of CO_2, a solution with no dissolved cations (i.e., where the partial pressure of CO_2 alone controlled the solution pH) would have a water to CO_2 ratio of approximately 1,430 and a pH of approximately 3.9 at a temperature of 20 °C. A solution saturated with a carbonate mineral (i.e., containing dissolved cations) would have a higher pH, would be able to hold a higher concentration of dissolved inorganic carbon (DIC), and would, therefore, have a lower ratio of water to CO_2. For example, saturation with siderite ($FeCO_3$) at pCO_2 of 1 bar requires 1.7×10^{-3} mol per liter of Fe^{2+}. This concentration of dissolved ferrous iron would increase the pH only to approximately 5.0 and decrease the water to CO_2 ratio to approximately 1,370 (from a value of 1,430 with no dissolved cations). Saturation with calcite, which is more soluble, would increase the pH to approximately 5.9 and decrease the water to CO_2 ratio to approximately 1,060. Thus, the $\delta^{18}O$ of carbonates precipitated from an aqueous solution formed at the surface of early Mars would be water-buffered. Under equilibrium conditions, the carbonates' $\delta^{18}O$ would be controlled by the processes affecting the $\delta^{18}O$ of the water, rather than by processes that fractionate the oxygen isotopes between species that comprise the DIC pool.

In the scenario described in the main text and shown in Fig. 3, a subsurface aqueous solution evaporates. The evaporation drives carbonate precipitation and CO_2 degassing. The distillative loss of water to evaporation and CO_2 to degassing cause an increase in the $\delta^{18}O$ and $\delta^{13}C$ of the residual fluid, respectively. In this system, the total dissolved inorganic carbon, DIC (in moles), can be expressed in two ways:

$$\mathrm{DIC} = pCO_2 \times K_H \times \left(1 + \frac{K_{A1}}{[H^+]} + \frac{K_{A1} \times K_{A2}}{[H^+]^2}\right) \times H_2O, \quad \text{[S4]}$$

$$\mathrm{DIC} = \frac{K_{SP}}{M^{2+}/H_2O} \times \left(1 + \frac{[H^+]}{K_{A2}} + \frac{[H^+]^2}{K_{A1} \times K_{A2}}\right) \times H_2O. \quad \text{[S5]}$$

Eq. **S4** describes equilibrium between the gas in the soil or rock pore space and the carbon in aqueous solution; Eq. **S5** describes saturation of a carbonate mineral, MCO_3. K_H, K_{A1}, K_{A2}, and K_{SP} are Henry's Law constant for CO_2, the first and second carbonic acid dissociation constants, and the solubility product constant for MCO_3, respectively (*SI Text* section *References for model constants*). $[H^+]$ is the concentration of the hydronium ion (in moles per liter), M^{2+} is the amount of the precipitating cation (in moles), H_2O is the amount of water (in liters), and pCO_2 is the pore CO_2 pressure (in atmospheres).

Equating these two expressions for DIC, we obtain

$$\frac{pCO_2 \times K_H \times K_{A1} \times K_{A2}}{[H^+]^2} = \frac{K_{SP}}{M^{2+}/H_2O}. \quad \text{[S6]}$$

Charge balance dictates

$$[H^+] - [OH^-] - [HCO_3^-] - 2 \times [CO_3^{2-}] + 2 \times \frac{M^{2+}}{H_2O} + A = 0, \quad \text{[S7]}$$

and, given carbonate species equilibrium, can be written as

$$[H^+] - \frac{K_W}{[H^+]} - \frac{pCO_2 \times K_H \times K_{A1}}{[H^+]} - 2 \times \frac{pCO_2 \times K_H \times K_{A1} \times K_{A2}}{[H^+]^2} + 2 \times \frac{M^{2+}}{H_2O} + A = 0. \quad \text{[S8]}$$

Here K_W is the dissociation constant of water and A is the total charge of nonprecipitating, conservative ions (in equivalents per liter). Rearranging Eq. **S6** to express M^{2+} as a function of $[H^+]$ and substituting this into Eq. **S8** yields a quartic equation for $[H^+]$, which has only one real, positive root and can be solved given pCO_2, A, and H_2O. After solving for $[H^+]$ this value can be used in Eq. **S6** to obtain the value of M^{2+} and in Eq. **S4** or **S5** to obtain the value of DIC.

Prescribing initial values for pCO_2, A, and H_2O and then progressively decreasing the amount of water to simulate an evaporating aqueous reservoir allows for all of the properties of the system to be solved as the water evaporates. As an amount of water, ΔH_2O, is lost,

$$H_2O_i = H_2O_{i-1} - \Delta H_2O, \quad \textbf{[S9]}$$

$$\Delta M^{2+} = M^{2+}_{i-1} - M^{2+}_i, \quad \textbf{[S10]}$$

where M^{2+}_{i-1} and M^{2+}_i are the amount of precipitating cation solved for with H_2O_{i-1} and H_2O_i liters of water, respectively. The total DIC loss is then

$$\Delta DIC = DIC_{i-1} - DIC_i = \Delta DIC_{carb} + \Delta DIC_{dgas} + \Delta DIC_{pres}, \quad \textbf{[S11]}$$

where DIC_{i-1} and DIC_i are the total DIC solved for with H_2O_{i-1} and H_2O_i liters of water, respectively. The subscripts *carb*, *dgas*, and *pres* denote, respectively, DIC loss to carbonate precipitation, distillative CO_2 transport to the surface, and an increase in pore pCO_2. The amount of carbon lost to carbonate precipitation is equal to the amount of precipitating cation lost (Eq. **S12**), and the rest is divided between distillative CO_2 loss and pore pressure increase,

$$\Delta DIC_{carb} = \Delta M^{2+}, \quad \textbf{[S12]}$$

$$\Delta DIC_{dgas} = f_{dgas} \times (\Delta DIC - \Delta DIC_{carb}), \quad \textbf{[S13]}$$

$$\Delta DIC_{pres} = (1 - f_{dgas}) \times (\Delta DIC - \Delta DIC_{carb}). \quad \textbf{[S14]}$$

Here f_{dgas} is a modulating factor that defines how much of the carbon loss in excess of carbonate precipitation is transported toward the surface as opposed to increasing the pressure in the pores. The pore pCO_2 then evolves as

$$pCO_{2_i} = pCO_{2_{i-1}} + \frac{\Delta DIC_{pres} \times N_A \times k_B \times T}{V}, \quad \textbf{[S15]}$$

where N_A is Avogadro's constant, k_B is Boltzmann's constant, T is the temperature, and V the pore space volume not occupied by aqueous solution, which increases as the water evaporates. If f_{dgas} is equal to 1, then there is no change in pressure, pH, and precipitating ion concentration (although the total amount of precipitating ion decreases as the solution loses water). If f_{dgas} is less than 1, then the pore pressure increases, pH decreases, and the concentration of precipitating cation at carbonate mineral saturation increases (though its total amount progressively decreases). As mentioned in the main text, we find that a value of f_{dgas} of approximately 0.9 best accounts for the coevolution of carbon and oxygen isotopic composition, the systematics of which are described below. That is, approximately 90% of the degassed CO_2 is transported to the surface and approximately 10% goes to increase the pore CO_2 pressure.

In a completely confined system, where water initially occupies all of the available pore space, the pCO_2 will increase until the solution becomes undersaturated with the carbonate mineral, at which time precipitation will cease. In a system that remains saturated (or supersaturated) and gradually loses CO_2 from pores that are overpressured with respect to the atmosphere, such as the environment we describe here, it is necessary only to have enough initial water-free pore space so as not to reach geologically unreasonable pressures. Even if we define the water in this system to occupy 90% of the initial available pore space, the resulting pressure increase for the required value of f_{dgas} is at most 20% of the original pressure—a very modest value. Though it might be reasonable to consider a pore space nearly completely saturated with water and an increase in pressure greater than 20%, prescribing the water to occupy more than 90% of the available pore space results in numeric instability of the model.

The processes that remove water and DIC from the system described above also fractionate the isotopes of oxygen and carbon, resulting in coevolution of the isotopic composition. The relationship observed among the carbonate $\delta^{18}O$, $\delta^{13}C$, and Δ_{47} indicates isotopic equilibrium between the water and DIC. Therefore, we reequilibrate the oxygen isotopic composition between the water and DIC at every model step. The preequilibration isotopic composition of the water and DIC reservoirs is

$${}^{18}R_i^{H_2O} \times H_2O_i = {}^{18}R_{i-1}^{H_2O} \times H_2O_{i-1} - \Delta H_2O \times {}^{18}R_{evap}, \quad \textbf{[S16]}$$

$${}^{18}R_i^{DIC} \times DIC_i = {}^{18}R_{i-1}^{DIC} \times DIC_{i-1} - \Delta DIC_{carb} \times {}^{18}R_{carb} - \Delta DIC_{dgas} \times {}^{18}R_{dgas} - \Delta DIC_{pres} \times {}^{18}R_{pres}, \quad \textbf{[S17]}$$

$${}^{13}R_i^{DIC} \times DIC_i = {}^{13}R_{i-1}^{DIC} \times DIC_{i-1} - \Delta DIC_{carb} \times {}^{13}R_{carb} - \Delta DIC_{dgas} \times {}^{13}R_{dgas} - \Delta DIC_{pres} \times {}^{13}R_{pres}, \quad \textbf{[S18]}$$

where ${}^{18}R_i^x$ is the ratio of ^{18}O to ^{16}O in reservoir x at step i and ${}^{13}R_i^x$ is the ratio of ^{13}C to ^{12}C in reservoir x at step i. The isotope ratios associated with the various loss processes depend on the fractionation factor (α) between the water and DIC pools and the mass being lost. The fractionation factors used in our model are shown in *SI Text* section 5.1.

The isotopic composition of water and CO_2 lost to transport toward the surface depends on whether diffusion limits the rate of this transport. If diffusion is not rate-limiting, ${}^{18}R_{evap} = {}^{18}R_{i-1}^{H_2O} \times {}^{18}\alpha_{vap\text{-}liq}$—the isotopic ratio of water vapor in equilibrium with the liquid. Similarly, ${}^{18}R_{dgas} = {}^{18}R_{i-1}^{DIC} \times {}^{18}\alpha_{CO_{2(g)}\text{-}DIC}$ and ${}^{13}R_{dgas} = {}^{13}R_{i-1}^{DIC} \times {}^{13}\alpha_{CO_{2(g)}\text{-}DIC}$. Diffusive transport imparts an additional fractionation α_{diff}, which is multiplied by the values of R shown above and depends on the relative masses of the CO_2 and H_2O isotopologues.

After modification of the isotopic ratios, the system is isotopically equilibrated at every simulation step. For carbon

$${}^{13}R_i^{DIC} = f_i^{CO_2(aq)} \times {}^{13}R_i^{CO_2(aq)} + f_i^{H_2CO_3} \times {}^{13}R_i^{H_2CO_3} + f_i^{HCO_3^-} \times {}^{13}R_i^{HCO_3^-} + f_i^{CO_3^{2-}} \times {}^{13}R_i^{CO_3^{2-}}, \quad \textbf{[S19]}$$

where

$$f_i^{CO_2(aq)} = \frac{1}{(1 + K_1 + \frac{K_{A1}}{[H^+]} + \frac{K_{A1} \times K_{A2}}{[H^+]^2})}, \quad \textbf{[S20]}$$

$$f_i^{H_2CO_3} = \frac{K_1}{(1 + K_1 + \frac{K_{A1}}{[H^+]} + \frac{K_{A1} \times K_{A2}}{[H^+]^2})}, \quad \textbf{[S21]}$$

$$f_i^{HCO_3^-} = \frac{\frac{K_{A1}}{[H^+]}}{(1 + K_1 + \frac{K_{A1}}{[H^+]} + \frac{K_{A1} \times K_{A2}}{[H^+]^2})}, \quad \textbf{[S22]}$$

$$f_i^{CO_3^{2-}} = \frac{\frac{K_{A1}\times K_{A2}}{[H^+]^2}}{(1 + K_1 + \frac{K_{A1}}{[H^+]} + \frac{K_{A1}\times K_{A2}}{[H^+]^2})}. \quad \textbf{[S23]}$$

The carbonate species are in isotopic equilibrium:

$$^{13}R_i^{CO_2(aq)} = {}^{13}R_i^{HCO_3^-} \times {}^{13}\alpha_{CO_2(aq)\text{-}HCO_3^-}, \quad \textbf{[S24]}$$

$$^{13}R_i^{H_2CO_3} = {}^{13}R_i^{HCO_3^-} \times {}^{13}\alpha_{H_2CO_3\text{-}HCO_3^-}, \quad \textbf{[S25]}$$

$$^{13}R_i^{CO_3^{2-}} = {}^{13}R_i^{HCO_3^-} \times {}^{13}\alpha_{CO_3^{2-}\text{-}HCO_3^-}. \quad \textbf{[S26]}$$

Eqs. **S19** and **S24** through **S26** can be solved for the carbon isotopic composition of all of the carbonate species. For oxygen, water is included in the equilibrium. The total number of moles of oxygen in the solution is

$$H_2O_i(55.5556 + 2\times[CO_2(aq)] + 3\times[H_2CO_3] + 3\times[HCO_3^-] + 3\times[CO_3^{2-}]), \quad \textbf{[S27]}$$

$$[CO_2(aq)] = f_i^{CO_2(aq)} \times \frac{DIC}{H_2O_i}, \quad \textbf{[S28]}$$

$$[H_2CO_3] = f_i^{H_2CO_3} \times \frac{DIC}{H_2O_i}, \quad \textbf{[S29]}$$

$$[HCO_3^-] = f_i^{HCO_3^-} \times \frac{DIC}{H_2O_i}, \quad \textbf{[S30]}$$

$$[CO_3^{2-}] = f_i^{CO_3^{2-}} \times \frac{DIC}{H_2O_i}. \quad \textbf{[S31]}$$

The oxygen isotopic ratio of the full system is

$$^{18}R_i^{TOT} = \frac{H_2O_i}{O_{TOT}} \times [55.5556 + 2\times f_i^{CO_2(aq)} \times {}^{18}R_i^{CO_2(aq)} + \ldots + 3\times(f_i^{H_2CO_3} \times {}^{18}R_i^{H_2CO_3} + f_i^{HCO_3^-} \times {}^{18}R_i^{HCO_3^-} + f_i^{HCO_3^{2-}} \times {}^{18}R_i^{HCO_3^{2-}})], \quad \textbf{[S32]}$$

and the oxygen isotopic ratios of the carbonate species are in equilibrium with that of the water are

$$^{18}R_i^{CO_2(aq)} = {}^{18}R_i^{H_2O} \times {}^{18}\alpha_{CO_2(aq)\text{-}H_2O}, \quad \textbf{[S33]}$$

$$^{18}R_i^{H_2CO_3} = {}^{18}R_i^{H_2O} \times {}^{18}\alpha_{H_2CO_3\text{-}H_2O}, \quad \textbf{[S34]}$$

$$^{18}R_i^{HCO_3^-} = {}^{18}R_i^{H_2O} \times {}^{18}\alpha_{HCO_3^-\text{-}H_2O}, \quad \textbf{[S35]}$$

$$^{18}R_i^{CO_3^{2-}} = {}^{18}R_i^{H_2O} \times {}^{18}\alpha_{CO_3^{2-}\text{-}H_2O}. \quad \textbf{[S36]}$$

Eqs. **S32** through **S36** can be solved for the oxygen isotopic ratios of all of the aqueous components.

In all of the above calculations, we neglect the effect of salinity on the activities of the different dissolved species and on the isotopic fractionations. We also neglect the effect of aqueous complexes on the activities of the dissolved species. Under the conditions that we explored, the absence of these effects introduces little error, as the ionic strength of the solution does not exceed 0.05 in most of the simulations, corresponding to a minimal water activity coefficient of approximately 0.998. The reason for this is that the concentration of the precipitating cations and the carbonate species are limited by the solubility of carbonate minerals. A negligible concentration of non-carbonate-forming ions in solution (e.g., SO_4^{2-}, Cl^-, K^+, Na^+) is justified by the observation that additional (noncarbonate) salts are absent from ALH84001 (8, 9).

In the model, we used the carbonate mineral siderite ($FeCO_3$) to limit the solubility of precipitating cations and DIC. The fractionations between siderite and water and between siderite and DIC were used to evolve the isotopic composition of the system. This choice is supported by X-ray diffraction and infrared spectra of the carbonates in ALH84001 (6), but below we also show that the results are fairly insensitive to the specific carbonate mineralogy.

5.1 References for model constants. We use the following equilibrium constants and isotopic fractionation factors (equilibrium fractionation factors except where noted otherwise).

1.	K_W	Water dissociation constant	(ref. 10)
2.	K_H	CO_2 Henry's Law constant	(ref. 10)
3.	K_1	True carbonic acid acidity constant	(ref. 10)
4.	K_{A1}	First carbonic acid dissociation constant	(ref. 11)
5.	K_{A2}	Second carbonic acid dissociation constant	(ref. 12)
6.	$K_{SP\text{-siderite}}$	Siderite solubility product constant	(ref. 13)
7.	$^{18}\alpha_{siderite\text{-}H_2O}$	Siderite-water O isotope fractionation factor	(ref. 14)
8.	$^{13}\alpha_{siderite\text{-}CO_2}$	Siderite-water C isotope fractionation factor	(ref. 14)
9.	$^{18}\alpha_{CO_2(aq)\text{-}H_2O}$	CO_2(aq)-water O isotope fractionation factor	(ref. 15)
10.	$^{13}\alpha_{CO_2(aq)\text{-}CO_2(g)}$	CO_2(aq)-CO_2(g) C isotope fractionation factor	(ref. 16)
11.	$^{18}\alpha_{HCO_3^-\text{-}H_2O}$	HCO_3^--water O isotope fractionation factor	(ref. 15)
12.	$^{13}\alpha_{HCO_3^-\text{-}CO_2(g)}$	HCO_3^--CO_2(g) C isotope fractionation factor	(ref. 16)
13.	$^{18}\alpha_{CO_3^{2-}\text{-}H_2O}$	CO_3^{2-}-water O isotope fractionation factor	(ref. 15)
14.	$^{13}\alpha_{CO_3^{2-}\text{-}CO_2(g)}$	CO_3^{2-}-CO_2(g) C isotope fractionation factor	(ref. 16)
15.	$^{18}\alpha^{eq}_{ice\text{-}H_2O}$	Ice-water O isotope fractionation factor	(ref. 17)
16.	$^{18}\alpha_{ice\text{-}H_2O}$	Kinetic ice-water O isotope fractionation factor	(ref. 18)
17.	$^{18}\alpha_{enstatite\text{-}H_2O}$	Enstatite-water O isotope fractionation factor	(ref. 19)
18.	$^{18}\alpha^{acid}_{siderite\text{-}H_2O}$	Siderite-water acid digestion O isotope fractionation factor	(ref. 20)

5.2 Sensitivity analysis. The model parameters are temperature, f_{dgas}, initial pCO_2, A, and V. Temperature is constrained by our clumped isotope measurements to be approximately 18 °C. Fig. S6 shows the sensitivity of the system to the other parameters. The sensitivity analysis was done for the default parameter values of $T = 20 \pm 5$ °C, $f_{dgas} = 0.9$, $pCO_2 = 0.6$ bar, $A = 0$ mol liter^{-1}, and $V = 90\%$ (of the total pore volume). In each case one of the model parameters was varied over a wide range of values and the others left at their default values. The model is highly sensitive only to the value of f_{dgas}—a prescribed fraction of the ratio of degassing to precipitation that would be calculated from carbonate chemistry. Physically, this parameter captures the competing rates of carbonate mineral precipitation and carbon loss from the subsurface regolith. A ratio smaller than unity reflects an environment where carbonate precipitation is rapid enough such that loss of carbon from the regolith pores to the surface cannot keep up. Because the continuation of carbonate saturation and precipitation requires that carbon is lost from aqueous solution, the CO_2 that does not leave the system goes to increase the pressure in the pore space that is unoccupied by the aqueous solution.

We also tested the sensitivity of the modeled $\delta^{18}O$-$\delta^{13}C$ covariation to the carbonate mineralogy. The mineralogy affects the chemistry of the aqueous solution (the solubility product constant affects the concentration precipitating cations, the pH, DIC speciation, and gas-aqueous partitioning) as well as the isotopic fractionation associated with carbonate mineral precipitation. Fig. S6*D* reveals that the choice of carbonate mineralogy (e.g., $FeCO_3$ versus $CaCO_3$) has only a minor impact on the isotopic composition of the precipitates.

5.3 Exploration of alternative scenarios. As mentioned in the model description (*Isotopic Evolution Model*), the $\delta^{18}O$ of the carbonates is buffered by oxygen isotope exchange between the DIC and the water and is, therefore, affected by the processes that fractionate oxygen isotopes in the water. Of these processes we find that only evaporation or vapor-phase diffusion can explain the observed increase in carbonate $\delta^{18}O$ over the course of concretion growth (Fig. 4 of the main text). Observed values of $\alpha_{ice\text{-}water}$ vary between the equilibrium value of 1.00291 and a kinetic fractionation factor of 1.00480 (18). Freezing, therefore, depletes the remaining water in ^{18}O, rather than enriching it and is also inconsistent with the measured temperatures of carbonate growth. Likewise, at the observed temperatures (including error) and considering the uncertainty in the measured oxygen isotopic composition of the orthopyroxene in ALH84001 [$\delta^{18}O_{SMOW}$ of 4.9 ± 1.5‰; (6)], oxygen isotope equilibrium between the water and the coexisting silicates can explain carbonate $\delta^{18}O_{SMOW}$ values only as high as approximately 19‰, inconsistent with the full observed range. Furthermore, equilibrium with the silicates would erase the atmospherically derived $\Delta^{17}O$ in ALH84001 carbonates.

In addition to the existence of mass-anomalous oxygen and sulfur isotope signatures in ALH84001, we argue that the initial $\delta^{18}O$ and $\delta^{13}C$ are inconsistent with a deep (magmatic or metamorphic) source for the fluids. If the water came from deeper within the crust, it is expected that the higher temperatures and longer exposure to silicates in the Martian crust would lead to oxygen isotopic equilibrium between the water and the rock. This is inconsistent with the carbonates' initial $\delta^{18}O$—at the measured temperature, carbonates precipitated from water in equilibrium with the silicates would have an initial $\delta^{18}O$ that is more than 10‰ higher than the lowest value observed in the concretion cores ($\delta^{18}O_{SMOW} \sim 5$‰; Fig. S7). As for the CO_2, based on the $\delta^{13}C$ of carbonates in the meteorite Zagami, the $\delta^{13}C_{PDB}$ of the magmatic Martian CO_2 has been argued to be lower than −20‰ (21). At the measured temperature, carbonates in equilibrium with this CO_2 would have $\delta^{13}C_{PDB} \sim -9$‰, more than 30‰ lower than the lowest observed values in the concretion cores (approximately 20–25‰). We note, however, that this estimate of Martian magmatic $\delta^{13}C$ is not well constrained.

Reliability of Temperature Determination.

1. Resetting of Clumped Isotopic Composition During Recrystallization. The clumped isotopic composition (and the associated temperature) need not always reflect the conditions of original carbonate formation. During diagenetic recrystallization or later exposure to aqueous conditions the carbonates can exchange oxygen isotopes with the water and reach a clumping equilibrium that reflects the temperature of diagenesis or alteration. Electron backscatter diffraction (EBSD) crystal orientation maps of the carbonate concretions reveal a pattern expected from the radial growth of nodules from pore fluids, indicating that the carbonates in ALH84001 have not recrystallized since their ingrowth (Fig. S4). Exchange without recrystallization is unlikely based on the coupled carbon and oxygen isotopic gradient between the concretion cores and rims. Because carbon and oxygen isotopic compositions of carbonate are modified by diagenetic processes differently, it is unlikely that two such processes conspired to produce the observed covariation of $\delta^{18}O$ and $\delta^{13}C$ across the very large range of values seen in ALH84001 carbonates.

2. Mixing Between Two End Members. Mixing in Δ_{47} space is nonlinear (22). If two end members have $\delta^{18}O$ and $\delta^{13}C$ that are sufficiently different (as do the cores and rims of the ALH84001 carbonates), their mixing can yield Δ_{47} values that are much higher than the end member Δ_{47} and apparent temperatures that are much lower. For our reliable Δ_{47} measurements (*Microvolume Measurements, Standardization, and Error Estimates*), if the end members formed at the same temperature but differed in bulk isotopic composition, as the ALH84001 carbonates do, then a best fit of a mixing model to the data yields a temperature of approximately 137.6 °C (Fig. S5*C*). We consider three possible end-member mixing processes that can conspire to give a low apparent temperature of approximately 20 °C.

First, the true distribution of carbonate could be bimodal in chemical and isotopic composition, with end members having Mg contents, $\delta^{18}O$ and $\delta^{13}C$ similar to the very centers of the cores and to the outermost concretion rims (Fig. S5*A*). If the distribution of chemical and isotopic compositions sampled by bulk acid digestion is different from the true distribution, it could yield spurious Δ_{47} temperature estimates. However, in situ, microscale measurements of chemical and isotopic composition of the carbonates do not reveal two physical end members.

The existence of two chemical end-member aqueous solutions can be rejected on the basis of the time scales for oxygen isotopic equilibration in aqueous solution as a function of pH and temperature. Essentially, the carbonates would have to precipitate after the mixing the two end members but before oxygen isotopic equilibrium (and consequently Δ_{47} equilibrium) was reached. The time to 99% equilibration as a function of pH and temperature is shown in Fig. S5*D*. The results of this calculation at temperatures exceeding 50 °C are less reliable because the equilibrium constants in the carbonate system have more uncertainty at these temperatures. They do, however, give a sense of the time scales required for almost full isotopic equilibrium. If the temperature was indeed approximately 137.6 °C, the carbonates would have to precipitate in a matter of seconds. We find this scenario unlikely.

A third possibility is that the acid digestion preferentially sampled the tails of a distribution of chemical and isotopic composition like that observed in ALH84001 (Fig. S5*B*). Physical mixing of the two gases evolved in this way in the absence of an aqueous solution in which they could approach Δ_{47} equilibrium would yield a spuriously low apparent temperature. However, we digested the carbonate for a total of 12 h at 90 °C—long

enough to extract all of the carbonate based on the dissolution kinetics of carbonates of different cations (23). Indeed, the carbonate yield during the last reaction step (4–12 h) was about a fifth of the first step (0–1 h) and second step (1–4 h). This gives confidence that almost all of the carbonate had been extracted and so even if mixing explains the results of steps 1 and 2, it cannot explain the results of step 3, which are similar to steps 1 and 2. Furthermore, based on the known correlation of $\delta^{18}O$ and $\delta^{13}C$ with Mg content, preferential dissolution of the end-member compositions requires that magnesian carbonates were extracted early in the digestion, which is discordant with their relative dissolution kinetics.

1. Huntington KW, et al. (2009) Methods and limitations of 'clumped' CO_2 isotope (Δ_{47}) analysis by gas-source isotope ratio mass spectrometry. *J Mass Spectrom* 44:1318–1329.
2. Eiler JM, Kitchen N, Rahn TA (2000) Experimental constraints on the stable-isotope systematics of CO_2 ice/vapor systems and relevance to the study of Mars. *Geochim Cosmochim Acta* 64:733–746.
3. Farquhar J, Thiemens MH, Jackson T (1998) Atmosphere-surface interactions on Mars: $\Delta^{17}O$ measurements of carbonate from ALH 84001. *Science* 280:1580–1582.
4. Leshin LA, McKeegan KD, Carpenter PK, Harvey RP (1998) Oxygen isotopic constraints on the genesis of carbonates from Martian meteorite ALH84001. *Geochim Cosmochim Acta* 62:3–13.
5. Saxton JM, Lyon IC, Turner G (1998) Correlated chemical and isotopic zoning in carbonates in the Martian meteorite ALH84001. *Earth Planet Sci Lett* 160:811–822.
6. Eiler JM, Valley JW, Graham CM, Fournelle J (2002) Two populations of carbonate in ALH84001: Geochemical evidence for discrimination and genesis. *Geochim Cosmochim Acta* 66:1285–1303.
7. Niles PB, Leshin LA, Guan Y (2005) Microscale carbon isotope variability in ALH84001 carbonates and a discussion of possible formation environments. *Geochim Cosmochim Acta* 69:2931–2944.
8. Treiman AH (1995) A petrographic history of Martian meteorite ALH84001—2 shocks and an ancient age. *Meteoritics* 30:294–302.
9. Mittlefehldt DW (1994) ALH84001, a cumulate orthopyroxenite member of the Martian meteorite clan. *Meteoritics* 29:214–221.
10. Zeebe RE, Wolf-Gladrow DA (2001) CO_2 *in Seawater: Equilibrium, Kinetics, Isotopes* (Elsevier, Amsterdam), p xiii.
11. Millero FJ, Graham TB, Huang F, Bustos-Serrano H, Pierrot D (2006) Dissociation constants of carbonic acid in seawater as a function of salinity and temperature. *Mar Chem* 100:80–94.
12. Hiscock WT, Millero FJ (2006) Alkalinity of the anoxic waters in the Western Black Sea. *Deep Sea Res Part 2 Top Stud Oceanogr* 53:1787–1801.
13. Benezeth P, Dandurand JL, Harrichoury JC (2009) Solubility product of siderite ($FeCO_3$) as a function of temperature (25–250 °C). *Chem Geol* 265:3–12.
14. Carothers WW, Adami LH, Rosenbauer RJ (1988) Experimental oxygen isotope fractionation between siderite-water and phosphoric-acid liberated CO_2-siderite. *Geochim Cosmochim Acta* 52:2445–2450.
15. Beck WC, Grossman EL, Morse JW (2005) Experimental studies of oxygen isotope fractionation in the carbonic acid system at 15°, 25°, and 40 °C. *Geochim Cosmochim Acta* 69:3493–3503.
16. Zhang J, Quay PD, Wilbur DO (1995) Carbon-isotope fractionation during gas-water exchange and dissolution of CO_2. *Geochim Cosmochim Acta* 59:107–114.
17. Lehmann M, Siegenthaler U (1991) Equilibrium oxygen-isotope and hydrogen-isotope fractionation between ice and water. *J Glaciol* 37:23–26.
18. Horita J (2009) Isotopic evolution of saline lakes in the low-latitude and polar regions. *Aquat Geochem* 15:43–69.
19. Zheng YF (1993) Calculation of oxygen isotope fractionation in anhydrous silicate minerals. *Geochim Cosmochim Acta* 57:1079–1091.
20. Rosenbaum J, Sheppard SMF (1986) An isotopic study of siderites, dolomites and ankerites at high temperatures. *Geochim Cosmochim Acta* 50:1147–1150.
21. Jull AJT, Eastoe CJ, Cloudt S (1997) Isotopic composition of carbonates in the SNC meteorites, Allan Hills 84001 and Zagami. *J Geophys Res* 102:1663–1669.
22. Eiler JM, Schauble E (2004) $^{18}O^{13}C^{16}O$ in Earth's atmosphere. *Geochim Cosmochim Acta* 68:4767–4777.
23. Al-Aasm IS, Taylor BE, South B (1990) Stable isotope analysis of multiple carbonate samples using selective acid extraction. *Chem Geol* 80:119–125.

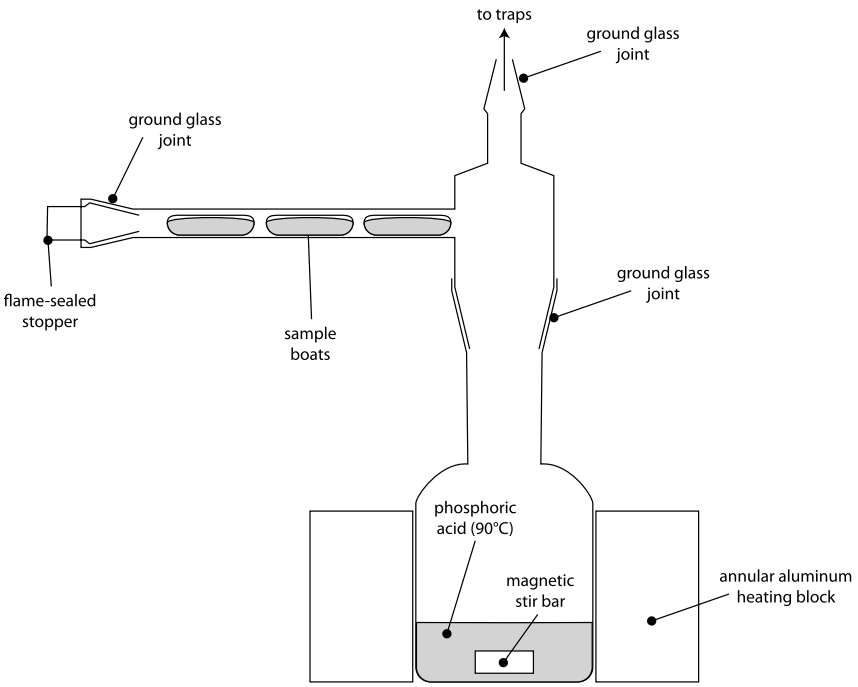

Fig. S1. Experimental apparatus. Crushed bulk ALH84001 was loaded into glass boats and placed in the glass side arm protruding (*Left*). A glass-coated magnet was placed behind (to the left of) the sample boats. Phosphoric acid (102%) was placed in the bottle, along with a Teflon-coated magnetic stir bar. Apiezon H vacuum grease was used on all of the ground glass joints to seal the reaction vessel and the apparatus was pumped on for more than 16 h (at a heating block temperature of 105 °C) to get rid of water. Before the digestion, the heating block temperature was lowered to 90 °C and given enough time to reach this temperature. The glass-coated magnet was used to push the sample boats into the acid and start the digestion. The CO_2 was continuously collected in liquid nitrogen after passing through a coiled glass trap held at −75 °C (ethanol-dry ice slush).

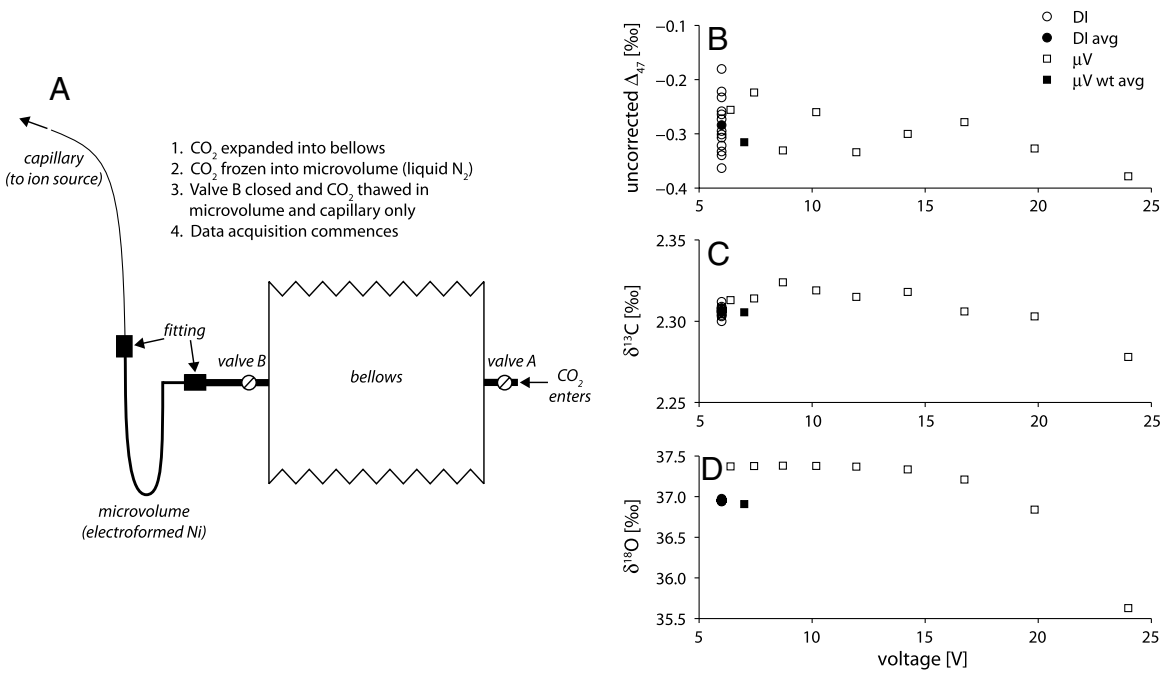

Fig. S2. Microvolume schematic and comparison of results with dual-inlet measurements of the same gas. (*A*) The microvolume. The CO_2 is frozen from the bellows into the small electroformed nickel U trap by immersion in liquid N_2. Valve B is then closed, the liquid N_2 removed, and the microvolume bathed in hot air in order for the CO_2 to thaw (this takes less than 30 s). The CO_2 flows down the pressure gradient in the capillary tube into the ion source. (*B*) Raw Δ_{47} (uncorrected for mass spectrometer artifacts and compositional dependence on δ_{47}) plotted against measurement voltage (on the faraday cup measuring mass 44 CO_2). The corrected Δ_{47} is always positive and slightly elevated relative to the true known value, for reasons discussed in *SI Text*. (*C*) $\delta^{13}C$ plotted against voltage. (*D*) $\delta^{18}O$ plotted against measurement voltage. In all three plots, unfilled and filled circles are the individual dual-inlet measurements and their average, respectively. Unfilled squares are the microvolume measurements and filled squares are their voltage-weighted average, plotted at a voltage of 7 V for ease of comparison with the dual-inlet measurements. The $\delta^{18}O$ and $\delta^{13}C$ are well-captured by the voltage-weighted average, whereas the Δ_{47} is systematically lower and closer to the true known value of Δ_{47} for these carbonate standards.

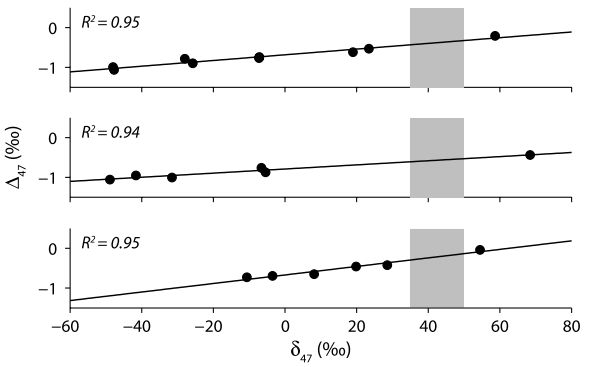

Fig. S3. Δ_{47} versus δ_{47} for gases of variable bulk isotopic composition heated to 1,000 °C to achieve a random distribution of the heavy isotopes. These gases should all have $\Delta_{47} = 0‰$, and it is not entirely clear why they do not. However, it has been established that a sample's true value of Δ_{47} is retrieved if the measured value is corrected by the δ_{47}-dependent amount represented by a fit to these δ_{47}–Δ_{47} data. Here we show that over the range of δ_{47} observed in ALH84001 carbonates (approximately 35–50‰; gray shaded areas), the relationship between δ_{47} and Δ_{47} of heated gases (and therefore the correction) is linear. The three subfigures show the "heated gas lines" for three different measurement periods (December 23–31, 2005; November 18, 2005; and February 18–24, 2006). We thank Weifu Guo, who performed these analyses, for the data.

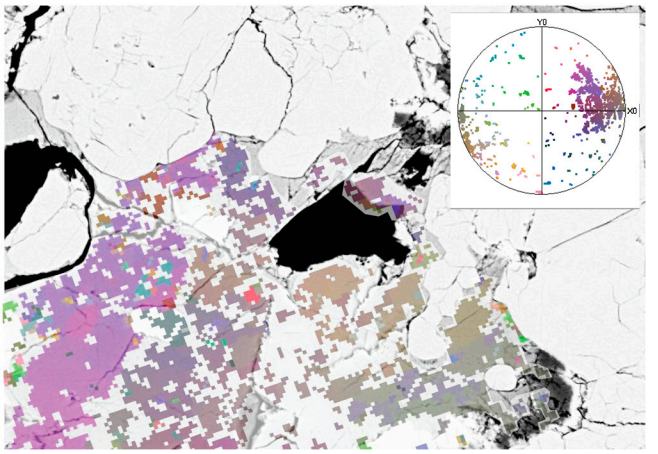

Fig. S4. Electron backscatter diffraction image of a carbonate concretion from the same split of ALH84001 from which we extracted carbonates for clumped isotope analysis. (*Inset*) The orientation of the carbonate *c* axis sweeping in a fan-like manner, consistent with radial growth of the concretion. Recrystallization would appear as a juxtaposition of crystal domains with an orientation of the carbonate *c* axis that is uncorrelated between adjacent domains. The absence of such a pattern indicates that the carbonates in ALH84001 have not recrystallized since their formation.

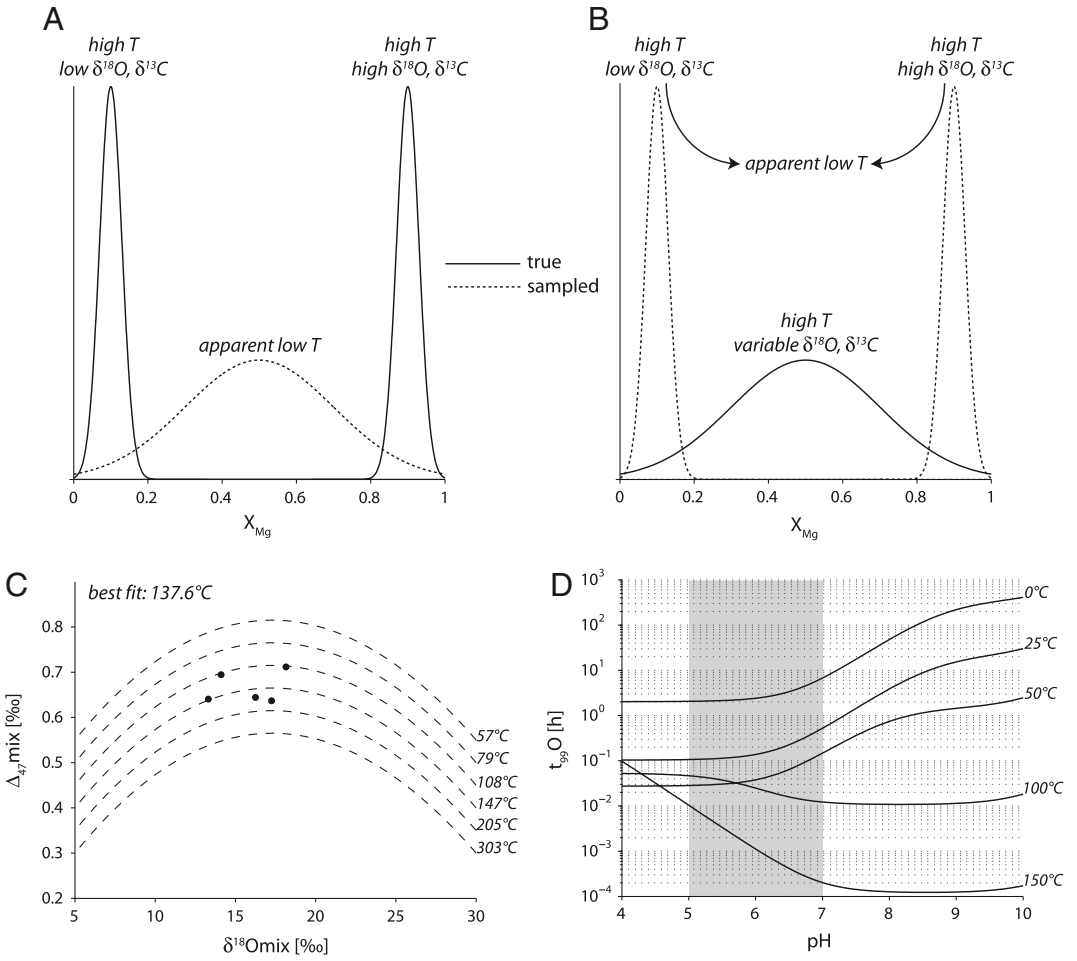

Fig. S5. The effect of two end-member mixing on the measured Δ_{47}. Schematic models for (*A*) physical or chemical mixing and (*B*) mixing during acid digestion of two end members with different $\delta^{18}O$ and $\delta^{13}C$ (and Mg content) and identical formation temperatures (and Δ_{47}). See *Mixing Between Two End Members* for details. (*C*) The Δ_{47} of a mixture of two end members with $\delta^{18}O_{SMOW}$ of 5 and 30‰, and $\delta^{13}C_{PDB}$ of 20 and 65‰, similar to the bulk isotopic composition of the concretion cores and rims, respectively. Our reliable analyses (*Microvolume Measurements, Standardization, and Error Estimates*) are best fit by a mixture of these two isotopic end members that formed at a temperature of 137.6 °C. Mixtures of end members formed at other temperatures (dashed lines) are compared to the data (filled circles). (*D*) The time to 99% oxygen isotope equilibration as a function of temperature and pH. Kinetic rate constants for the relevant reactions are from ref. 10. Equilibration proceeds more rapidly at high temperature, though we note that the equilibrium constants in the carbonate system are best constrained at temperatures below 50 °C with the calculations at higher temperatures more uncertain. The gray rectangle brackets the range of pH reached in our calculations, which is a function of the partial pressure of CO_2 and the initial nonprecipitating ion load. At the best fit mixing temperature (approximately 137.6 °C, Fig. S5*C*), the carbonates would have to precipitate on a time scale of seconds for oxygen isotope (and Δ_{47}) equilibrium not to be reached—that is, to sustain the spuriously low apparent temperatures due to end-member mixing.

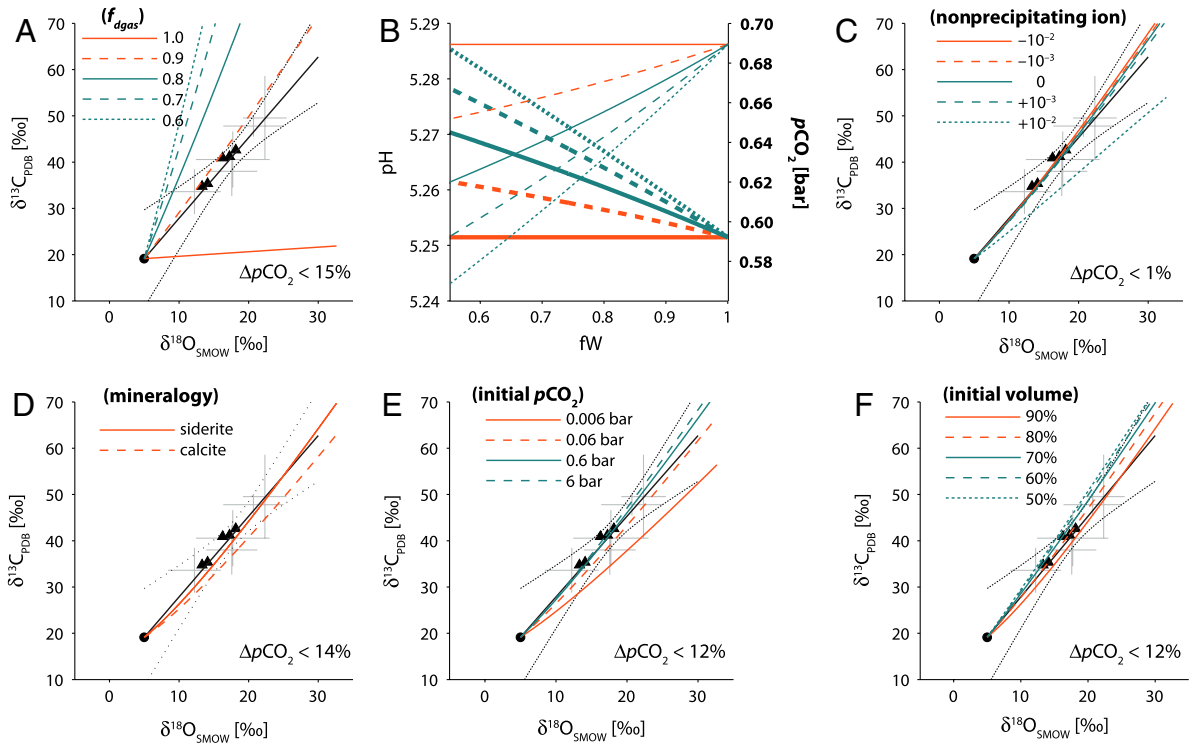

Fig. S6. Model sensitivity analysis. In all cases the sensitivity of the modeled $\delta^{13}C$ and $\delta^{18}O$ evolution to the value of a single parameter is shown. We demonstrate the sensitivity of the pore pCO_2 increase and the pH decrease only to the value of f_{dgas}, but give the maximal increase in pore pCO_2 on the lower right of each subfigure. (*A*) Sensitivity to the value of f_{dgas}, the fraction of noncarbonate carbon lost to transport toward the surface (the rest goes to increase the pore pCO_2). The model results are sensitive to the value of this parameter because the ratio of degassing to precipitation determines the net fractionation of carbon isotopes. Carbonate mineral precipitation depletes the remaining DIC, whereas CO_2 degassing enriches it in ^{13}C. (*B*) Sensitivity of the pCO_2 increase (thick lines, right *y* axis) and pH decrease (thin lines, left *y* axis) to the value of f_{dgas}. The line styles and colors correspond to the legend in *A*. A low value of f_{dgas} results in the largest increase in pore pCO_2, but still less than a 15% increase. (*C*) Sensitivity to the initial charge due to the concentration of nonprecipitating, conservative ions (parameter *A*). (*D*) Sensitivity to carbonate mineralogy, represented in the model by the value of K_{SP} and of the fractionation factors between the carbonate mineral and the water and CO_2 from which it formed. (*E*) Sensitivity to initial pCO_2. (*F*) Sensitivity to the initial volume of pore space occupied by the aqueous solution (the rest of the volume is available for gaseous CO_2).

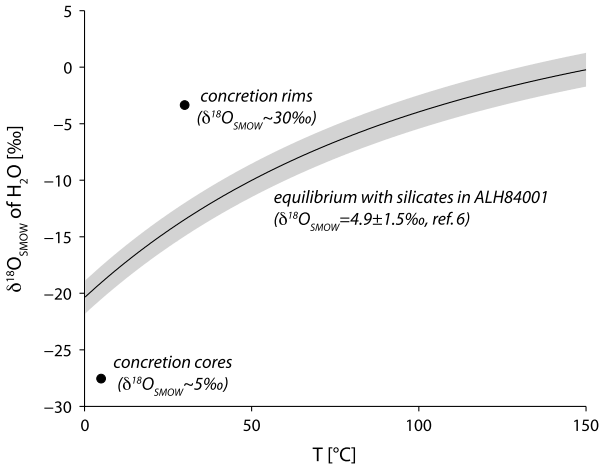

Fig. S7. Comparison of the $\delta^{18}O$ of water in equilibrium with the observed range of carbonate $\delta^{18}O$ to that of water in equilibrium with the silicates in ALH84001 at 20 °C. The carbonates start out too ^{18}O-depleted and end up too enriched in ^{18}O for oxygen isotope exchange between the water and rock to explain the core to rim evolution of $\delta^{18}O$. In addition, the low $\delta^{18}O$ of the carbonates (relative to the expectation from equilibrium with the silicates in ALH84001) suggests that the water from which the carbonates precipitated did not come from deeper within the Martian crust, but from the surface environment.

Table S1. Correction to $\delta^{18}O$, $\delta^{13}C$, and Δ_{47} measured from the microvolume

Period	Standard*	Weight, mg	$\Delta\delta^{18}O$, ‰	$\Delta\delta^{13}C$, ‰	$\Delta\Delta_{47}$, ‰
Ext. B	CM	6.9	−0.007	−0.009	0.002
	CM	6.9	−0.061	−0.086	0.018
	CM	7.1	−0.169	−0.085	0.008
	CM	3.9	−0.153	−0.082	0.014
	CM	3.9	−0.239	−0.113	0.045
	TV	7.1	−0.288	−0.108	0.008
	ID	2.5	—	—	0.031
	ID	4.5	0.181	−0.019	−0.023
	correction		**−0.092**	**−0.063**	**0.015**
	95% error†		**±0.281**	**±0.072**	**±0.039**
Ext. C	CM	4.7	0.163	0.000	0.056
	CM	4.4	−0.101	−0.027	0.042
	CM	4.0	−0.035	−0.028	0.047
	CM	4.7	−0.073	−0.003	0.037
	CM	4.2	−0.116	0.001	0.057
	CM	4.7	−0.056	0.005	0.048
	CM	4.1	−0.041	0.000	0.050
	TV	4.5	−0.061	0.004	0.025
	TV	4.1	0.000	0.003	0.054
	TV	4.5	−0.039	0.001	0.015
	CM	4.5	−0.046	0.001	0.044
	CM	3.4	—	—	0.063
	CM	3.5	—	—	0.078
	correction		**−0.037**	**−0.004**	**0.047**
	95% error†		**±0.159**	**±0.024**	**±0.027**

*The internal standards used for determination of the correction were Carrera Marble (CM), a travertine (TV), and Inyo Dolomite (ID). The standards cover a range of D47 between 0.352 and 0.662‰.

†95% confidence interval error estimate after application of the correction.

Table S2. All results, including aliquot A

Aliquot A

Type	$\delta^{18}O_U$‰	$\delta^{18}O_C$‰	$\delta^{13}C_U$‰	$\delta^{13}C_C$‰	Δ_{47U}‰	Δ_{47C}‰	$N_{>7V}$	Err. 1: stds	Err. 2: stat	T °C
				Step 1 (0–1 h)						
μV	13.05	—	35.52	—	0.556	—	4	—	0.044	55^{+20}_{-16}
				Step 2 (1–4 h)						
μV	16.68	—	40.87	—	0.522	—	2	—	0.068	69^{+40}_{-28}
				Step 3 (4–12 h)						
μV	18.96	—	40.82	—	—	—	0	—	—	—

Aliquot B

Type	$\delta^{18}O_U$‰	$\delta^{18}O_C$‰	$\delta^{13}C_U$‰	$\delta^{13}C_C$‰	Δ_{47U}‰	Δ_{47C}‰	$N_{>7V}$	Err. 1: stds	Err. 2: stat	T °C
				Step 1 (0–1 h)						
DI	13.23	—	34.54	—						
μV	13.29	13.38 ± 0.28	34.54	34.60 ± 0.07	0.657	0.642	5	0.039	0.036	27^{+13}_{-11}
				Step 2 (1–4 h)						
DI	16.86	—	40.99	—						
μV	17.23	17.32 ± 0.28	40.98	41.05 ± 0.07	0.653	0.638	5	0.039	0.034	28^{+13}_{-11}
				Step 3 (4–12 h)						
μV	17.90	17.99 ± 0.28	40.87	40.94 ± 0.07	0.757	0.742	1	0.039	0.098	3^{+25}_{-19}

Aliquot C

Type	$\delta^{18}O_U$‰	$\delta^{18}O_C$‰	$\delta^{13}C_U$‰	$\delta^{13}C_C$‰	Δ_{47U}‰	Δ_{47C}‰	$N_{>7V}$	Err. 1: stds	Err. 2: stat	T °C
				Step 1 (0–1 h)						
DI	14.07	—	35.12	—						
μV	14.08	14.11 ± 0.16	35.14	35.14 ± 0.02	0.740	0.693	8	0.027	0.024	14^{+7}_{-6}
				Step 2 (1–4 h)						
DI	16.33	—	40.67	—						
μV	16.23	16.27 ± 0.16	40.67	40.67 ± 0.02	0.690	0.643	9	0.027	0.022	26^{+8}_{-7}
				Step 3 (4–12 h)						
μV	18.13	18.17 ± 0.16	42.38	42.39 ± 0.02	0.758	0.711	7	0.027	0.028	10^{+7}_{-6}

The columns from left to right are measurement type (DI = dual-inlet, μV = microvolume), uncorrected $\delta^{18}O$, corrected $\delta^{18}O$ with error (see Table S1), uncorrected $\delta^{13}C$, corrected $\delta^{13}C$ with error, uncorrected Δ_{47}, corrected Δ_{47}, number of acquisitions, Δ_{47} error estimated from carbonate standards, Δ_{47} counting statistics error, temperature with error. Details of error estimation are in *SI Text* section *Microvolume Measurements, Standardization, and Error Estimates*.